coatings

MDPI

Article

Structural, Morphological and Optical Properties of Nanostructured ZrO_2 Films Obtained by an Electrochemical Process at Different Deposition Temperatures

Konstantin Lovchinov [1], Rositsa Gergova [2] and Gergana Alexieva [3,*]

[1] Acad. J. Malinowski Institute of Optical Materials and Technologies, Bulgarian Academy of Sciences, Acad. G. Bonchev Str., Bld. 109, 1113 Sofia, Bulgaria; lovchinov@iomt.bas.bg
[2] Central Laboratory of Solar Energy and New Energy Sources, Bulgarian Academy of Sciences, 72 Tsarigradsko Chaussee, 1784 Sofia, Bulgaria; rgergova@phys.bas.bg
[3] Faculty of Physics, Department of General Physics, University of Sofia, 5 James Bourchier Blvd., 1164 Sofia, Bulgaria
* Correspondence: gerry@phys.uni-sofia.bg

Abstract: This article focuses on the impact of the deposition temperature (in the range from 60 to 80 °C) in ZrO_2 films obtained by the electrochemical deposition process on SnO_2-covered glass substrates. The solution in which the deposition takes place is aqueous, containing $ZrOCl_2$ with a concentration of 3×10^{-5} M and KCl with a concentration of 0.1 M. By implementing X-ray diffraction (XRD), optical profilometry, scanning electron microscopy (SEM), and UV-VIS-NIR spectroscopy, the temperature dependence of ZrO_2 films properties was revealed. The X-ray Diffraction XRD spectra showed six different diffraction maxima ((−111)M, (101)T, (111)M, (112)M, (202)M, and (103)M) associated with the electrochemical ZrO_2 layers, and the polycrystalline structure of the films was confirmed at all deposition temperatures. The determination of the average roughness did not indicate significant temperature dependence in the deposited layers. SEM micrographs showed that the layers were composed of grains, most of them of a regular shape, although their size increased slightly with an increased deposition temperature. The coarsest-grained structure was observed for the layers deposited at 80 °C. It was demonstrated that the deposition temperature weakly impacts the reflectance and transmittance spectra of the ZrO_2 layers. Such layers with low values of specular and high values of diffuse transition, and reflection in the spectral range from 380 to 800 nm, can be applied to various optoelectronic devices such as thin-film solar cells.

Keywords: electrochemical deposition; surface morphology; ZrO_2 films; optical measurement

Citation: Lovchinov, K.; Gergova, R.; Alexieva, G. Structural, Morphological and Optical Properties of Nanostructured ZrO_2 Films Obtained by an Electrochemical Process at Different Deposition Temperatures. *Coatings* **2022**, *12*, 972. https://doi.org/10.3390/coatings12070972

Academic Editor: Saulius Kaciulis

Received: 8 June 2022
Accepted: 4 July 2022
Published: 8 July 2022

1. Introduction

Metal oxide nanostructured materials are traditional but increasingly relevant subject of many scientific and technological researches. Recently, zirconium dioxide (ZrO_2) nanomaterials have attracted considerable scientific interest due to their inherent combination of properties such as high mechanical and thermal resistances, chemical inertness, high corrosion resistance, high refractive index, wide range of optical transparency (UV–Vis–IR region), and good dielectric constant [1–7]. Also known as "zirconia," zirconium dioxide is a wide-bandgap n-type metal oxide semiconductor with high ionic conductivity [8–10]. ZrO_2 is a ceramic material. At atmospheric pressure, it occurs in three phases depending on the formation temperature: monoclinic (below 1170 °C), tetragonal (between 1170 °C and 2370 °C), and cubic (above 2370 °C) [11].

Because of its unique combination of electronic and mechanical properties, ZrO_2 proves to be a promising material for use in many applications including gas sensors [12,13], solar cells [14], dental implant materials [15], fuel cells [16,17], etc.

A considerable number of research articles report ZrO_2 structures obtained by different methods, such as the following: sol–gel method [18], magnetron sputtering [19,20],

chemical vapor deposition [21], electron beam physical vapor deposition (EBPVD) [22], laser ablation [23], hydrothermal method [24], and atomic layer deposition [25]. A key element in the design of zirconia nanostructures is the choice of technique and approach for their elaboration, which ensures the presence of needed properties and qualities, and predetermines specific applications. Therefore, in this research study, the emphasis was placed on the electrochemical technique and the influence of the deposition temperature (in the range from 50 to 80 °C) on properties of ZrO_2 thin films deposited on SnO_2-covered glass substrates. The electrochemical method can be applied to produce large areas with controlled and diverse morphology and size nanostructures. This method is quite inexpensive, and it does not require the use of complicated equipment.

In the presented manuscript, we report the results for structural, morphological, and optical properties of the nanostructured ZrO_2 films under investigation, amplifying the information already existing in the literature for similar layers produced by electrochemical deposition technique [26,27].

2. Materials and Methods

This section describes the method of deposition and the conditions under which it was carried out, as well as the specific equipment that was used to obtain the results of the research. The deposition of the zirconia layers was electrochemical and was carried out by means of three electrode cells located in a thermostatic bath (Figure 1). The deposition took place in an aqueous solution. Dissolved in this solution were $ZrOCl_2$, supplied by Alfa Aesar (98%, with concentration of 5 mM) and KCl supplied by Valerus Ltd. (99.5%, with concentration of 100 mM). Deposition was realized at different electrolyte temperatures in the range from 60 to 80 °C, and the potential between saturated calomel electrode (SCE) and substrate (cathode) was kept constant at -700mV. The sample in the solution is in thermodynamic equilibrium. The deposition time of all zirconia layers studied was 20 min.

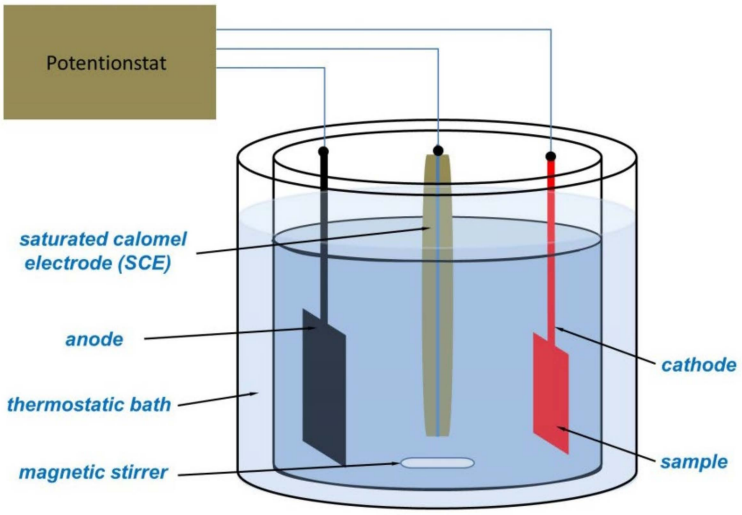

Figure 1. Schematic representation of the electrodes located in the electrochemical system.

A Philips (Amsterdam, The Netherlands) 1710D8 Advance diffractometer with CuKα radiation (instrumental broadening is 0.04° and λ = 1.54178 Å) was employed to determine X-ray diffraction (XRD, Philips, Amsterdam, The Netherlands) patterns in ZrO_2 layers. A Philips 515 scanning electron microscope (SEM, Philips, Amsterdam, The Netherlands) was used to observe the surface morphology of the deposited layers. The Zeta 20 3D optical profilometer (KLA, Milpitas, CA, USA) was used to determine the surface topography and average roughness (using the Zeta 3D_engr_1_8_5 software, KLA, Milpitas, CA, USA); the vertical resolution of the instrument was 1 nm. The measurements were performed at several different points on the surface of the ZrO_2 layers, each with an area of 6887 μm^2. The conductivity of the electrolyte was measured by BANTE 510 (Bante Instruments

Inc., Sugar Land, TX, USA). The spectra of transmittance and reflectance ((specular and diffuse component) and haze ratio) were obtained by a UV-VIS-NIR Shimadzu UV 3600 spectrophotometer (Shimadzu Scientific Instruments, Columbia, MD, USA).

3. Results and Discussion

The structure of the electrochemical layers of ZrO_2 deposited at different temperatures was determined by XRD analysis. The diffraction maxima are shown in Figure 2. The diffraction pattern of the substrate (SnO_2-covered glass) is shown with the black line for comparison. In the graph, we can distinguish six diffraction maxima related to zirconium dioxide; five of them are due to the monoclinic phase and one (which is the most intense) is due to the tetragonal phase. The diffraction maxima due to the SnO_2-covered glass substrate are marked with an asterisk (JCPDS No. 14–1445). The five maxima due to the monoclinic phase ((111), (112), (202), (013), and (−111)) are characteristic for ZrO_2 and are thoroughly described in the literature (JCPDS No. 37–1484) [28]. The diffraction maximum corresponding to the tetragonal direction (101) possesses the highest intensity (JCPDS No. 81–1544) [29]. This is relatively unusual for ZrO_2, because its crystallographic structure is monoclinic at deposition temperatures below 1170 °C. The explanation for this intense maximum may be related to epitaxial growth from the magnetron-sputtered SnO_2/glass substrate possessing tetragonal structure [30].

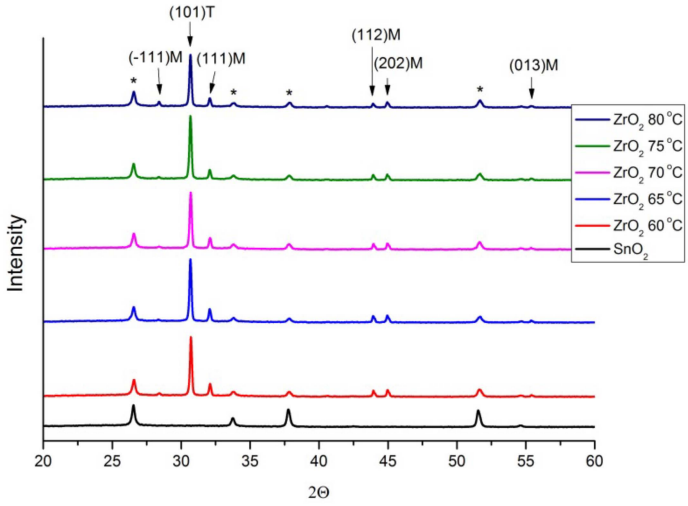

Figure 2. XRD patterns of the electrochemical ZrO_2 layers deposited on SnO_2 substrate at different temperatures. The diffraction maxima due to the SnO_2-covered glass substrate are marked with an asterisk (*).

Table 1 shows the positions of the diffraction maxima (2θ) and the values of the full width at half maximum (FWHM). From these diffraction maxima, the average grain size (D) was calculated using Scherrer's Equation (1) [31] for each crystallographic direction associated with a maximum:

$$D = (57.3 \times \lambda K)/(\beta \cos \theta), \quad (1)$$

where λ − (1.54178 Å) is the wavelength of CuK_1 radiation, θ is the Bragg angle, β is calculated from selected diffraction peak FWHM, and K is the particle shape factor (in most cases for particles with a predominantly regular shape it is assumed to be 0.9). There was no recognizable relationship between the calculation of the average grain size and the deposition temperature of the zirconia layers. We can note a slight decrease in the average grain size with the increase in the deposition temperature in the crystallographic directions with the greatest intensity of the diffraction maxima (101)T and (111)M. The missing results denoted with dash sign "-" in Table 1 were calculated with a large error due to the low intensity in the maxima in these directions, and for this reason, they were not shown.

Table 1. The position of the peak in the XRD patterns, 2θ, full width at half maximum (FWHM), β of 2θ, and the average grain sizes, D.

ZrO_2 Deposited on SnO_2 Substrate									
	(101)T			**(111)M**			**(112)M**		
	2Θ	**FWHM**	**D, (nm)**	**2Θ**	**FWHM**	**D, (nm)**	**2Θ**	**FWHM**	**D, (nm)**
60 °C	30.71	0.14	59	32.1	0.156	53	43.95	0.127	67
65 °C	30.68	0.151	54	32.08	0.162	51	43.95	0.230	37
70 °C	30.69	0.157	53	32.1	0.175	47	43.95	0.163	53
75 °C	30.68	0.160	52	32.07	0.165	50	43.93	0.146	59
80 °C	30.68	0.160	52	32.08	0.164	50	43.92	0.162	53
	(202) M			**(013) M**			**(−111)M**		
	2Θ	**FWHM**	**D, (nm)**	**2Θ**	**FWHM**	**D, (nm)**	**2Θ**	**FWHM**	**D, (nm)**
60 °C	44.99	0.190	45	55.41	0.116	77	-	-	-
65 °C	44.97	0.187	46	-	-	-	28.35	0.120	68
70 °C	44.99	0.254	34	-	-	-	28.67	0.162	51
75 °C	44.97	0.217	40	-	-	-	-	-	-
80 °C	44.96	0.197	44	-	-	-	28.40	0.118	70

Figure 3 shows the 3D optical profilometry in the electrochemical layers of ZrO_2 deposited at different temperatures. The RMS (root mean square) roughness values determined from the measurements are shown in Table 2. The RMS roughness in the SnO_2 substrate (magnetron sputtered on glass) is also presented for comparison. The calculations were made on the basis of data taken from three different sections (Sq^1, Sq^2, and Sq^3) of the surface of the samples, with each of them having an area of (97 μm × 71 μm = 0.69 mm^2). The results of optical profilometry did not show a noticeable relationship between the RMS roughness and the deposition temperature in the electrochemically deposited layers of ZrO_2. Here, the differences can be related to the different inhomogeneities in the layers, with the layer deposited at 65 °C (Figure 3c) possessing the greatest inhomogeneity. This inhomogeneity is not related to the substrate, as its RMS roughness is relatively constant and is at least twice lower than that in the deposited layers. The probable reason for the differences in the inhomogeneities at different temperatures is the different mobility of the ions in the solution, and the way they are attached to the substrate at each individual deposition temperature. Evidence of this is the electrolyte solution's changing conductivity with temperature; the data from the measurements in this parameter are shown in Table 3. Measurements show that as the electrolyte's temperature increases, the conductivity (σ) increases and resistivity (ρ) decreases.

Table 2. Average roughness in the ZrO_2 layers deposited at different temperatures on SnO_2 substrate.

	SnO_2 Substrate	**Electrochemical ZrO_2**				
		60 °C	65 °C	70 °C	75 °C	80 °C
Sq^1 (nm)	39	84	111	79	97	95
Sq^2 (nm)	34.5	82	119	76	95	87
Sq^3 (nm)	42.5	82	94	84	87	86
AVG (nm)	39 ± 2.7	83 ± 0.6	108 ± 8.2	79 ± 2.6	93 ± 3.4	89 ± 3

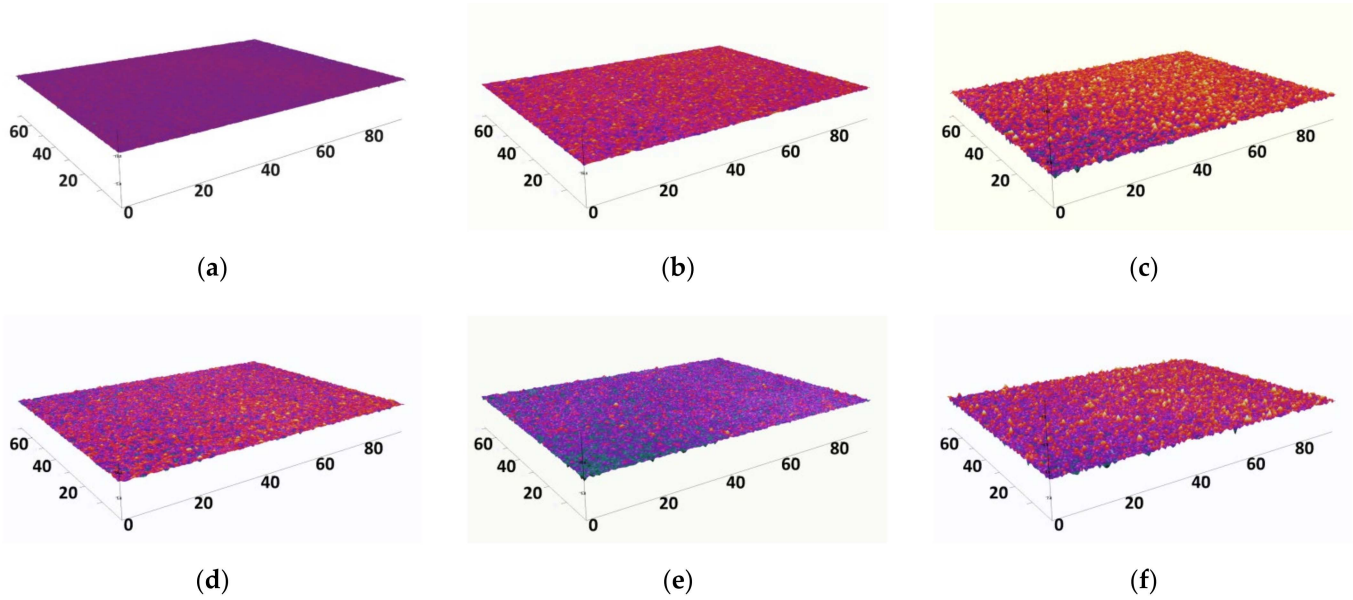

Figure 3. 3D optical profilometry images of SnO_2 substrate and electrochemically deposited ZrO_2 layers obtained at different temperatures for 20 min: SnO_2 substrate—(**a**); 60 °C—(**b**); 65 °C—(**c**); 70 °C—(**d**); 75 °C—(**e**); 80 °C—(**f**).

Table 3. Conductivity (σ) and resistivity (ρ) in electrochemical solutions measured at different temperatures.

	Electrochemical Solution				
Temperature	60 °C	65 °C	70 °C	75 °C	80 °C
σ–mS/cm	3.89	3.97	4.07	4.25	4.44
ρ–Ω/cm	257	252	246	235	225

The average thickness in the ZrO_2 layers deposited at different temperatures was measured with a 3D optical profilometer, and the results were: 60 °C—445 nm, 65 °C—517 nm, 70 °C—580 nm, 75 °C—595 nm, and 80 °C—480 nm.

Figure 4 shows the SEM micrographs of the magnetron-sputtered SnO_2 substrate on glass and the electrochemical layers of ZrO_2 deposited at different temperatures. The micrographs show that the zirconia layers have a predominantly granular structure with grain sizes of about 0.3–0.5 µm for the layers deposited at 60 °C (Figure 4b) and 1–2 µm for the layers deposited at 80 °C (Figure 4f). Here, in contrast to RMS's roughness, we can distinguish the dependence between the size of the grains located on the surface of the layers and the deposition temperature. With an increase in the deposition temperature, there was an evident increase in the size of the grains located on the surface of the electrochemical layers. The apparent shape of the grains of which the layers are composed is relatively regular. In Figure 4d, an onset of grain coalescence leading to the formation of larger crystallites is observed for the layer deposited at 70 °C. This layer appears to have the best morphology for the range of the deposition temperatures studied, and this can also be confirmed by the lowest-measured RMS roughness at this deposition temperature. This improved structure may be due to more favorable conditions, such as ion mobility and adhesion to the substrate, contributing to the formation of this type of structure.

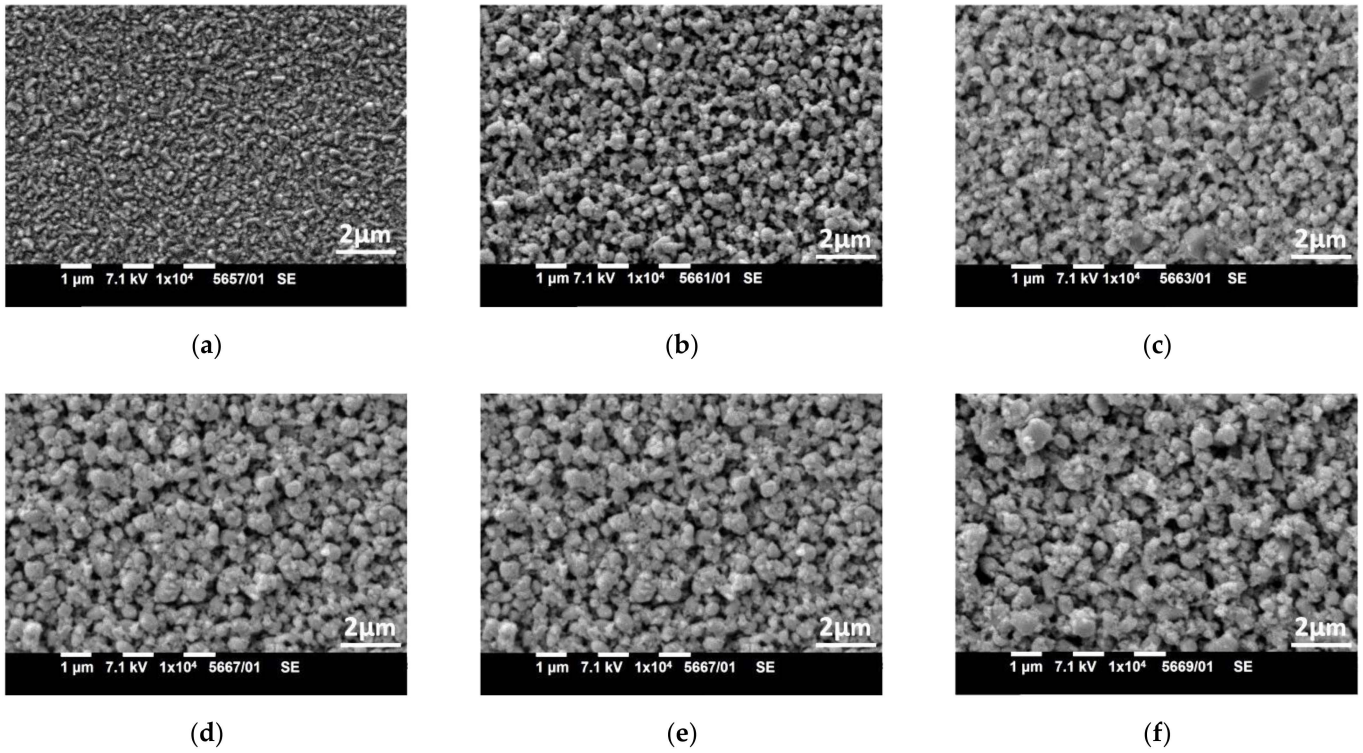

Figure 4. SEM micrograph of SnO_2 substrate and ZrO_2 layers electrochemically deposited at different temperatures for 20 min: SnO_2 substrate—(**a**); 60 °C—(**b**); 65 °C—(**c**); 70 °C—(**d**); 75 °C—(**e**); 80 °C—(**f**).

The transmission, diffuse transmission, and haze ratio spectra of zirconia layers deposited at different temperatures are shown in Figure 5. For comparison, the spectra of the SnO_2 substrate are also shown in Figures 5 and 6. In the transmission spectra we observe a decrease in the values (related to the specular component of it) (Figure 5a) with increasing deposition temperature up to 75 °C. Further increases in temperature up to 80 °C show a slight increase in the values. In the diffuse transmission spectra (Figure 5b), an increase in the values is observed with increasing deposition temperature, in which case the layer deposited at the highest temperature (80 °C) has the highest values. The most likely explanation for the higher values in specular transmission for the layer deposited at 80 °C, compared to those deposited at 70 °C and 75 °C, is due to its lesser thickness, which comes from the different deposition rates depending on the electrolyte temperature. At higher deposition temperatures (from 80 °C), we obtained the formation of larger grains than those of the layers deposited at 70 and 75 °C (Figure 4) but located with a lower density on the surface; the lower density leads to higher values in the specular transmission of this layer. In the case of diffuse transmission, the grain size is also important. We observed the highest values in the spectra for the layer deposited at 80 °C because this layer has the largest grains, which leads to greater scattering. The values calculated for the haze ratio (Figure 5c) show the highest values in the visible region of the layers deposited at 75 °C, followed by those at 70 °C. This is because these layers have the lowest values of specular transmission, and the haze ratio represents the percentage ratio of the diffuse component related to the full transmission.

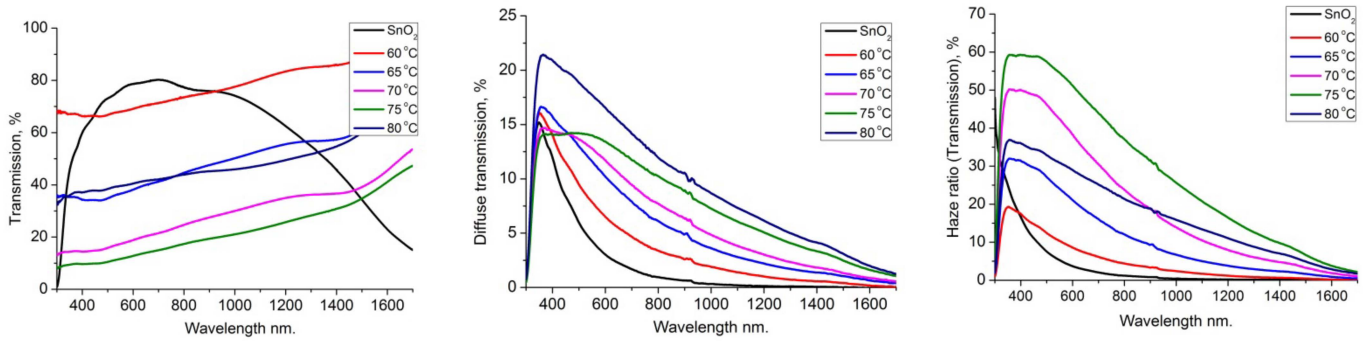

(**a**) (**b**) (**c**)

Figure 5. Transmittance (**a**), diffuse transmittance (**b**), and haze ratio (**c**) in ZrO_2 layers electrochemically deposited at different temperatures.

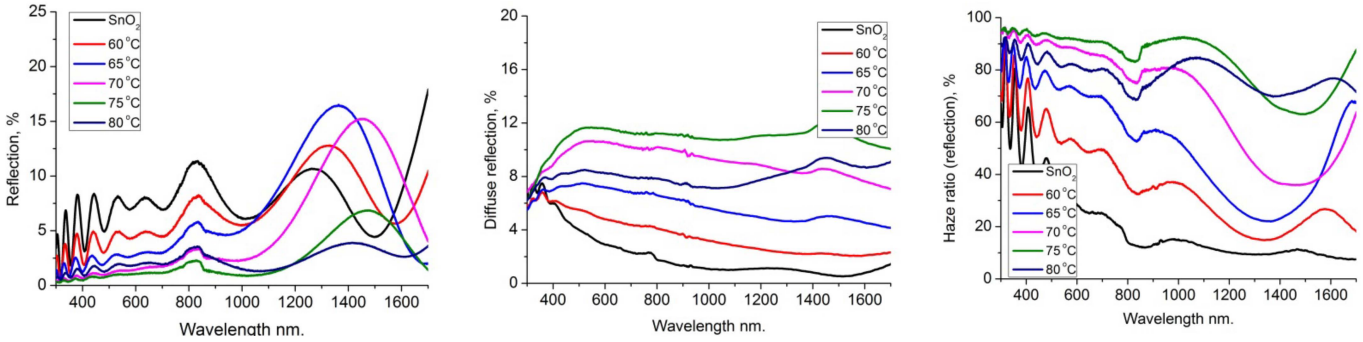

(**a**) (**b**) (**c**)

Figure 6. Reflectance (**a**), diffuse reflectance (**b**), and haze ratio (**c**) in ZrO_2 layers electrochemically deposited at different temperatures.

Figure 6 shows the optical spectra of reflection, diffuse reflection, and haze ratio of electrochemical ZrO_2 layers deposited at different temperatures. The spectra corresponding to the specular component of the reflection are shown in Figure 6a. Here, in general, the layers have very low values (less than 5%) in the visible range, and these values decrease with increasing deposition temperature to reach less than 1% for the layers deposited at 75 and 80 °C. Here, we observe strongly pronounced interference maxima that are a result of the SnO_2 substrate (magnetron sputtered on glass). This effect is observed when the layers are not thick and homogeneous enough and the substrate (which must have a flat parallel surface) is transparent to some extent and reflected through the layer. In the spectra of diffuse reflection (Figure 5b), the values are slightly higher than those of mirror reflection and reach about 10%–11% for the layers deposited at 70 and 75 °C. Unlike diffuse transmission, the layer deposited at 80 °C does not have the highest values, because in the reflection, apart from the size and shape of the grains, their surface density is also of great importance. For this reason, layers with more densely located grains on the substrate surface (such as layers deposited at 70 and 75 °C) have higher values in diffuse reflection. In diffuse reflection spectra, we do not observe interference maxima, because the SnO_2 substrate has negligibly small scattering values below 1%, which does not affect the electrochemical layers of ZrO_2. The values calculated for the haze ratio (Figure 6c) show high values in the visible range; as for the layers with a denser surface grain structure (those deposited at 70 and 75 °C), they reached 90%–95%. The "haze ratio" relationship is the percentage ratio of the components of diffuse transmission or reflection to the total transmission or reflection. The dependence of the optical spectra behavior on surface morphology is reported for ZrO_2 films obtained with different deposition

methods, reflecting the peculiarities of the selected deposition method, the experimental conditions, and the specific structural and dielectric properties of the films arising from them. In [32], ZrO_2 thin films were obtained by magnetron sputtering onto optical grade quartz substrates. The crystallite size of the layers was in the range from 5 to 25 nm and was shown to significantly affect the optical characteristics of the thin films. The increasing crystallite size is associated with a random distribution of the grains, which makes the film surface rough, and as a result, an increase in light-scattering losses was observed. In [20], the average crystallite size of zirconium oxide films prepared by the magnetron-sputtering process at different argon partial pressures increases from 19 nm to 25 nm with increasing pressure. The minimum transmission values above 63% were observed for all films deposited at different pressures, and the values increased slightly with increasing argon partial pressure. This is explained by the thickness decreasing from 433 nm to 385 nm. In [33], homogenous and transparent nanocrystalline zirconia layers deposited on quartz substrates were produced by thermal oxidation using DC magnetron-sputtering techniques. It is shown that by increasing the annealing time from 60 to 240 min, the grains combine and form larger grains, in this manner changing the surface morphology from a pyramidal to cluster-type surface. By increasing the annealing time, the transparency of the zirconia films also increased. ZrO_2 films were also deposited by filtered cathodic vacuum arc [34]. The film structure is amorphous at room temperature and develops to polycrystalline upon heating the substrates to temperatures of 150 °C and above. Increasing the temperature leads to an increase in the surface's roughness. It was shown that changes in the film microstructure result in variations in their optical properties. For ZrO_2 thin films deposited through plasma-enhanced atomic layer deposition [17], it was shown that the transmittance increased monotonically with increasing wavelength. The lowest transmittance of 76.6% was measured at 300 nm, and the highest transmittance of 95.5% was measured at 800 nm (~30 nm; substrate: borosilicate glass; deposition temperature: 150 °C). ZrO_2 films [5] spin-coated with a simple water-based solution and cured with UV-A radiation = 330 nm for different times (40, 80, and 120 min) were compared with thermally annealed film (at 350 °C). The UV-A radiation-exposed films, in comparison to thermal treatment, exhibited a decrease in optical transmittances. The optical spectroscopy results demonstrated that increased doses of UV-A radiation improved the quality of films, in comparison with heat-treated films. In comparison with most of the above cited papers [5,17,32–34], we observed a greater size of grains and greater value in film roughness, leading to greater values in diffuse and haze ratio spectra. In any case, all these features depend on the applied deposition method, as well as the variety and specificity of working conditions.

4. Conclusions

The innovation approach we used to produce zirconia thin films by an environmentally compatible and quite inexpensive electrochemical deposition enriches and amplifies the existing data for essential properties of ZrO_2 layers grown by other deposition methods. We described our results on the impact of deposition temperature on the structural, morphological, and optical properties of nanostructured ZrO_2 films. The XRD patterns showed six (one in the tetragonal phase and five in the monoclinic phase) different diffraction maxima related to zirconium oxide, with no relationship between the deposition temperature and the average grain size. The calculations obtained from the optical profilometry did not show a relationship between RMS roughness and the deposition temperature in the electrochemical layers of ZrO_2, as the differences can be related to the different inhomogeneities in the layers. SEM micrographs revealed that the layers were composed mainly of granular structures, and the constituent formations had relatively regular spherical shapes. The size of these formations increased with increasing deposition temperature, and at 80 °C, they were about 1–2 μm. We also observed dependence in the optical spectra, as the values of the specular components of transmission and reflection decreased with increasing deposition temperature, and the values of the diffuse components and the haze ratio increased. It was demonstrated that the electrochemical method, in a relatively narrow and easily achievable

temperature interval, allows the growth of diverse morphology and size nanostructures. Such layers of zirconia (with a wide energy band gap) with low values in specular and high values in diffuse transition and reflection in the visible and NIR range can be applied in some optoelectronic devices, such as background scatter layers in thin-film solar cells.

Author Contributions: Conceptualization, K.L.; methodology, K.L. and G.A.; software, K.L.; validation, G.A., R.G. and K.L.; formal analysis, G.A., R.G. and K.L.; investigation, K.L. and G.A.; resources, K.L.; data curation, K.L. and G.A.; writing—original draft preparation, K.L. and G.A.; writing—review and editing, G.A., R.G. and K.L.; visualization, K.L., R.G. and G.A.; supervision, K.L.; project administration, K.L.; funding acquisition, K.L. All authors have read and agreed to the published version of the manuscript.

Funding: This research paper is funded by the Bulgarian National Science Fund (BNSF) under the project КП–06–Н38/7 (12.2019).

Institutional Review Board Statement: Not applicable.

Informed Consent Statement: Not applicable.

Data Availability Statement: The authors confirm that the data supporting the findings of this study are available within the article.

Conflicts of Interest: The authors declare no conflict of interest. The funders had no role in the design of the study; in the collection, analyses, or interpretation of data; in the writing of the manuscript; or in the decision to publish the results.

References

1. Ravi Kumar, K.; Pridhar, T.; Sree Balajia, V.S. Mechanical properties and characterization of zirconium oxide (ZrO_2) and coconut shell ash (CSA) reinforced aluminium (Al 6082) matrix hybrid composite. *J. Alloys Compd.* **2018**, *765*, 171–179. [CrossRef]
2. Wang, L.; Cai, K.F.; Wang, Y.Y.; Yin, J.L.; Li, H.; Zhou, C.W. Preparation and characterization of tetragonal-ZrO_2 nanopowders by a molten hydroxides method. *Ceram. Int.* **2009**, *35*, 2499–2501. [CrossRef]
3. Wang, Y.; Zhou, X.; Liang, Z.; Jin, H. Characterization of Ultrasonic-Assisted Electrochemical Deposition of Ni-Co-ZrO_2. *Coatings* **2018**, *8*, 211. [CrossRef]
4. Lin, P.-C.; Lin, K.; Lin, Y.-H.; Yang, K.-C.; Semenov, V.I.; Lin, H.-C.; Chen, M.-J. Improvement of Corrosion Resistance and Biocompatibility of Biodegradable Mg–Ca Alloy by ALD $HfZrO_2$ Film. *Coatings* **2022**, *12*, 212. [CrossRef]
5. Bashir, A.; Farooq, M.; Malik, A.; Naseem, S.; Bhatti, A.S. UV-A Treatment of ZrO_2 Thin Films Fabricated by Environmental FriendlierWater-Based Solution Processing: Structural and Optical Studies. *Coatings* **2021**, *11*, 821. [CrossRef]
6. Melninkaitis, A.; Tolenis, T.; Mažulė, L.; Mirauskas, J.; Sirutkaitis, V.; Mangote, B.; Fu, X.; Zerrad, M.; Gallais, L.; Commandré, M.; et al. Characterization of zirconia– and niobia–silica mixture coatings produced by ion-beam sputtering. *Appl. Opt.* **2011**, *50*, 188–196. [CrossRef]
7. Pazhani, R.; Padma Kumar, H.; Varghese, A.; Moses Ezhil Raj, A.; Solomon, S.; Thomas, J.K. Synthesis, vacuum sintering and dielectric characterization of zirconia (t-ZrO_2) nanopowder. *J. Alloys Compd.* **2011**, *509*, 6819–6823. [CrossRef]
8. Deshmukh, S.B.; Bari, R.H.; Patil, G.E.; Kajale, D.D.; Jain, G.H.; Patil, L.A. Preparation and Characterization of Zirconia Based Thick Film Resistor as a Ammonia Gas Sensor. *Int. J. Smart Sens. Intell. Syst.* **2012**, *5*, 540–558. [CrossRef]
9. Deshmukh, S.B.; Bari, R.H. Nanostructured ZrO_2 Thin Films Deposited by Spray Pyrolysis Techniques for Ammonia Gas Sensing Application. *ILCPA* **2015**, *56*, 120–130. [CrossRef]
10. Hemalatha, E.; Gopalakrishnan, N. Synthesis of ZrO_2 nanostructure for gas sensing application. *Bull. Mater. Sci.* **2020**, *43*, 12. [CrossRef]
11. Bocanegra-Bernal, M.H.; Díaz de la Torre, S. Phase transitions in zirconium dioxide and related materials for high performance engineering ceramics. *J. Mater. Sci.* **2002**, *37*, 4947–4971. [CrossRef]
12. Husain, A.; Ahmad, S.; Mohammad, F. Thermally stable and highly sensitive ethene gas sensor based on polythiophene/zirconium oxide nanocomposites. *Mater. Today Commun.* **2019**, *20*, 100574. [CrossRef]
13. Hemalatha, E.; Gopalakrishnan, N. Gas sensing performances of pure and Cu-doped ZrO_2 nano structures. *Appl. Phys. A* **2019**, *125*, 493. [CrossRef]
14. Pai, A.R.; Nair, B. Synthesis and characterization of a binary oxide ZrO_2–TiO_2 and its application in chlorophyll dye-sensitized solar cell with reduced graphene oxide as counter electrodes. *Bull. Mater. Sci.* **2015**, *38*, 1129–1133. [CrossRef]
15. Ziębowicz, A.; Sambok-Kiełbowicz, A.; Walke, W.; Mzyk, A.; Kosiel, K.; Kubacki, J.; Bączkowski, B.; Pawlyta, M.; Ziębowicz, B. Evaluation of Bacterial Adhesion to the ZrO_2 Atomic Layer Deposited on the Surface of Cobalt-Chromium Dental Alloy Produced by DMLS Method. *Materials* **2021**, *14*, 1079. [CrossRef] [PubMed]
16. Minh, N.Q. Ceramic fuel cells. *J. Am. Ceram. Soc.* **1993**, *76*, 563–588. [CrossRef]

17. Oh, J.; Seo, G.; Kim, J.; Bae, S.; Park, J.-W.; Hwang, J.-H. Plasma-Enhanced Atomic Layer Deposition of Zirconium Oxide Thin Films and Its Application to Solid Oxide Fuel Cells. *Coatings* **2021**, *11*, 362. [CrossRef]
18. Lim, H.S.; Ahmad, A.; Hamzah, H. Synthesis of zirconium oxide nanoparticle by sol-gel technique. *AIP* **2013**, *1571*, 812. [CrossRef]
19. Kuo, D.H.; Chien, C.H. Growth and properties of sputtered zirconia and zirconia–silica thin films. *Thin Solid Film.* **2003**, *429*, 40–45. [CrossRef]
20. Patel, U.S.; Patel, K.H.; Chauhan, K.V.; Chawla, A.K.; Rawal, S.K. Investigation of Various Properties for Zirconium Oxide Films Synthesized by Sputtering. *Procedia Technol.* **2016**, *23*, 336–343. [CrossRef]
21. Sawka, A. Chemical Vapour Deposition of Scandia-Stabilised Zirconia Layers on Tubular Substrates at Low Temperatures. *Materials* **2022**, *15*, 2120. [CrossRef] [PubMed]
22. Tcheliebou, F.; Boulouz, M.; Boyer, A. Preparation of fine-grained MgO and Gd_2O_3 stabilized ZrO_2 thin films by electron beam physical vapor deposition co-evaporation. *J. Mater. Res.* **1997**, *12*, 3260–3265. [CrossRef]
23. Prieto-López, L.O.; Yubero, F.; Machorro, R.; De La Cruz, W. Optical properties of Zr and ZrO_2 films deposited by laser ablation. *Microelectron. J.* **2008**, *39*, 1371–1373. [CrossRef]
24. Wang, S.; Shen, J. Fabrication of sol–gel derived ZrO_2 thin film for HR coatings via rapid thermal annealing process. *J. Sol-Gel Sci. Technol.* **2013**, *67*, 339–343. [CrossRef]
25. Tang, L.; Maruyama, H.; Han, T.; Nino, J.C.; Chen, Y.; Zhang, D. Resistive switching in atomic layer deposited HfO_2/ZrO_2 nanolayer stacks. *Appl. Surf. Sci.* **2020**, *515*, 146015. [CrossRef]
26. Gal-Or, L.; Silberman, I.; Chaim, R. Electrolytic ZrO_2 Coatings: I. Electrochemical Aspects. *J. Electrochem. Soc.* **1990**, *138*, 1939. [CrossRef]
27. Lopes, N.I.A.; Freire, N.H.J.; Resende, P.D.; Santos, L.A.; Buono, V.T.L. Electrochemical deposition and characterization of ZrO_2 ceramic nanocoatings on superelastic NiTi alloy. *Appl. Surf. Sci.* **2018**, *450*, 21–30. [CrossRef]
28. Jafarpour, M.; Rezapour, E.; Ghahramaninezhad, M.; Rezaeifard, A. A novel protocol for selective synthesis of monoclinic zirconia nanoparticles as a heterogeneous catalyst for condensation of 1,2-diamines with 1,2-dicarbonyl compounds. *New J. Chem.* **2014**, *38*, 676–682. [CrossRef]
29. Sharifi, H.; Divandari, M.; Khavandi, A.; Idris, M.H. Effect of Al powder and silica sol on the structure and mechanical properties of Al_2O_3-ZrO_2 foams. *Acta Metall. Sin.* **2010**, *23*, 241–247. [CrossRef]
30. Lovchinov, K.; Slavov, L.; Alexieva, G.; Ivanov, P.; Marinov, G.; Gergova, R.; Strijkova, V.; Babeva, T. Study of ZrO_2 nanolayers deposited electrochemically on different conductive substrates. *Mater. Sci. Semicond. Process.* **2021**, *131*, 105843. [CrossRef]
31. Mass, J.; Bhattacharya, P.; Katiyar, R. Effect of high substrate temperature on Al-doped ZnO thin films grown by pulsed laser deposition. *Mater. Sci. Eng. B.* **2003**, *103*, 9–15. [CrossRef]
32. Ramana, C.V.; Vemuri, R.S.; Fernandez, I.; Campbell, A.L. Size-effects on the optical properties of zirconium oxide thin films. *Appl. Phys. Lett.* **2009**, *95*, 231905. [CrossRef]
33. Hojabri, A.; Pourmohammad, S. Optical Properties of Nano-Crystalline Zirconia Thin Films Prepared at Different Post-Oxidation Annealing Times. *Acta Phys. Pol. A* **2016**, *129*, 647–649. [CrossRef]
34. Zhao, Z.W.; Tay, B.K.; Huang, L.; Yu, G.Q. Study of the structure and optical properties of nanocrystalline zirconium oxide thin films deposited at low temperatures. *J. Phys. D Appl. Phys.* **2004**, *37*, 1701–1705. [CrossRef]